[22] J. L. Gimlett and N. K. Cheung, "Effects of Phase-To-Intensity Noise Conversion by Multiple Reflections on Gigabit Per Second DFB Laser Transmission Systems," IEEE JLT, Vol. 7, pp. 888-895, June, 1989.

[23] M. Tur, E. Shafir and K. Bloteijaer, "Source-induced noise in optical systems driven by low-coherence sources," IEEE JLT, Vol. 8, pp. 183-189, Feb. 1990.

[24] E. Goldstein and L. Eskildsen, "Scaling Limitations in Transparent Optical Netwokrs due to Low-Level Crosstalk," IEEE Photonics Technology Letters, Vol. 7, pp. 93-94, Jan. 1995.

[25] R. G. Waarts and R. -P. Braun, "System Limitation due to Four-Wave Mixing in Single Mode Optical Fiber, " Eletronics Letters, Vol. 22, pp. 873-875, July 1986.

[26] D. J. Blumenthal and N. C. Kothari, "Coherent Crosstalk in Multichannel FSK/DD Lightwave Systems Due to Four-Wave Mixing in Semiconductor Optical Amplifiers," IEEE Photonics Technology Letters, Vol. 8, No.1, pp. 133-135, Jan. 1996.

[27] D. J. Blumenthal, P. Granestrand and L. Thylen, "BER Floors due to Heterodyne Coherent Crosstalk in Space Photonic Switches for WDM Networks," IEEE Photonics Technology Letters, Vol. 8, No. 2, pp. 284-286, Feb. 1996.

Deflection Routing in Multihop Space-Division Optical Networks

Alberto Bononi

Dipartimento di Ingegneria dell'Informazione, Università di Parma, Viale delle Scienze I-43100 Parma, Italy

Abstract

Transparent multihop optical networks suffer from the accumulation from node to node of crosstalk and amplified spontaneous emission noise, which may severely degrade the quality of received signals. It is thus important to keep the number of intermediate hops as low as possible.

This paper compares two single-wavelength cell-switching space-division optical networks that employ deflection routing. The first has a well-known Manhattan Street (MS) distributed topology. The second has a centralized star topology: the star is a multistage space-division photonic switch with limited buffers. Deflected packets delivered to the wrong user are transparently re-routed to the star.

In both networks, as the network load increases, the crosstalk level per hop increases, as well as the number of crossings caused by deflections. The traffic statistics hence strongly affect the quality of the received signals.

A simple frequency sweeping technique is shown to effectively reduce the signal-crosstalk beat, thus allowing network operation with switch crosstalk factors as low as -20 dB.

It is found that a distributed topology like MS is not scalable in terms of both throughput/delay and transmission quality, and the centralized topology should be preferred.

1 Introduction

A major advantage of transparent optical networks is the possibility of flexibly upgrading transmission rates and hence network capacity by upgrading only transmitters and receivers at the access nodes, leaving the core of the network untouched. Such an advantage in management is also a major weakness in transmission. Transparency implies non-regenerative transmission from source to destination, with the ensuing degradation of the quality of signals due to accumulation of noise and distortion.

Amplified spontaneous emission (ASE) noise and device-induced coherent crosstalk are the two major transmission impairments in high-speed transparent optical local area networks [1].

In a cell-switching environment with dynamic routing, it is essential that cell paths be limited to a small number of hops, since each hop entails large power losses, accumulation of ASE and crosstalk. Thus topologies that have on average a few hops are ideal candidates for transparent networks employing deflection routing. Here we compare a Manhattan Street (MS) optical network to a Centralized Network.

2 Network Model

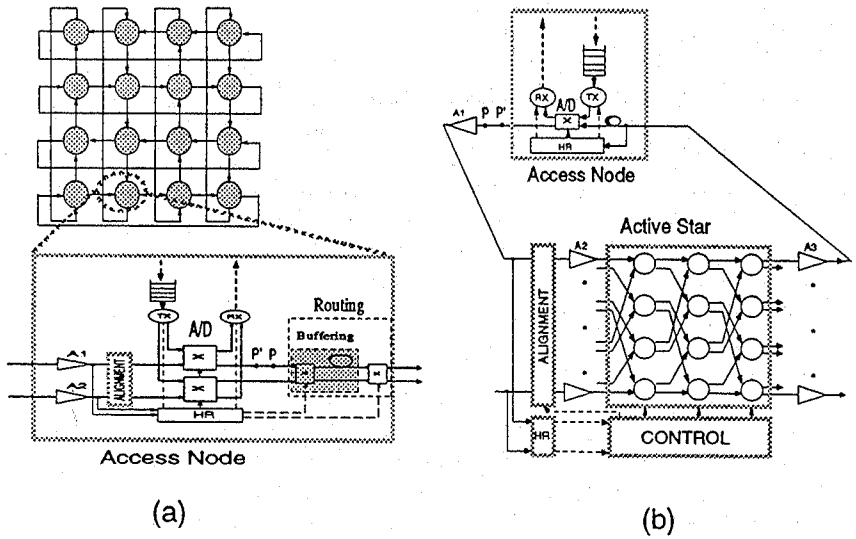

Fig. 1. (a) Distributed optical network (MS); (b) Centralized optical network (CN)

The two space-division optical networks that will be compared in this paper are shown in Fig. 1:

(a) – The first is a two-connected distributed optical MS network with M nodes. Each node is equipped with two add-drop optical crossbar switches (A/D), an optical transmitter (TX) and an optical receiver (RX), and has an electronic input buffer to store incoming cells. Cells are aligned at the node by tunable optical delays (alignment stage). The header recognition block (HR) taps power off to electronically read the cell headers and make alignment/add-drop/routing decisions.

The routing block is either composed of a single crossbar (*1c*), or has a buffering stage composed of a second crossbar and a one-cell fiber delay loop (*2c*), and is driven by a shortest-path deflection routing algorithm [2]. Deflection routing [3] is used because en-route transparent optical buffering cannot easily be provided, since, as we will show, it introduces large power losses and crosstalk. Nodes without buffers and with a single buffer per node only will be considered, since it is known that in uniform traffic a single buffer is enough to route packets almost as efficiently as with infinitely many buffers [4].

(b) – The centralized network (CN) is composed of an MxM space-division cell switch (Active Star) to which M access nodes are connected by dedicated fibers. Each access node is similar to the one in (a), but only one optical input/output is present, and only the add-drop part is provided.

The routing function is concentrated at the active star, where cells are aligned by tunable optical delays. The active star is a complete multistage photonic switch, with $\log_2 M$ Shuffle-Exchange (SX) stages based on crossbar directional couplers.

The elementary 2x2 routing elements within the active star (shown with circles in Fig. 1(b)) are either of type 1c or 2c like the routing block of the node in (a).

Although the routing is physically centralized, the control is distributed to allow scalability at high speed. Each routing element is controlled based only on the destinations of packets at its inputs (and possibly present in its buffer) using deflection routing. Deflected packets are delivered to the wrong user and transparently re-routed to the interconnect. The network, which is intrinsically single-hop, becomes gradually multi-hop as deflections take place because of the internal blocking of the interconnect.

2.1 Teletraffic

Suppose the offered traffic is uniform, i.e., each node receives from the outside a stream of independent packets uniformly destined to all other nodes in the network. Let the average arrival rate at each node be T packets/slot. At most one packet can be injected in the optical layer per slot, and packets from the input fiber(s) are given priority over local packets. As long as the input electronic buffers are not saturated, T coincides with the throughput per node. Let u be the link utilization, i.e., the probability that a slot from a link carries a packet. Given the symmetry of our networks, u is the same for all slots.

If H is the number of hops (i.e., *access node crossings*) that a packet on average undergoes before reaching its destination, a simple application of Little's law gives:

$$T = \frac{k\,u}{H}. \qquad (1)$$

where k is the in/out degree of the access node, $k = 1$ for CN, and $k =$ MS.

For a given u, reducing H as the positive effect of increasing the sustained throughput T. The weakly-multihop CN should then allow a much higher throughput than the strongly-multihop MS. Equivalently, for the same sustained throughput, CN should have a much lower slot utilization u, which has the positive effect of decreasing crosstalk.

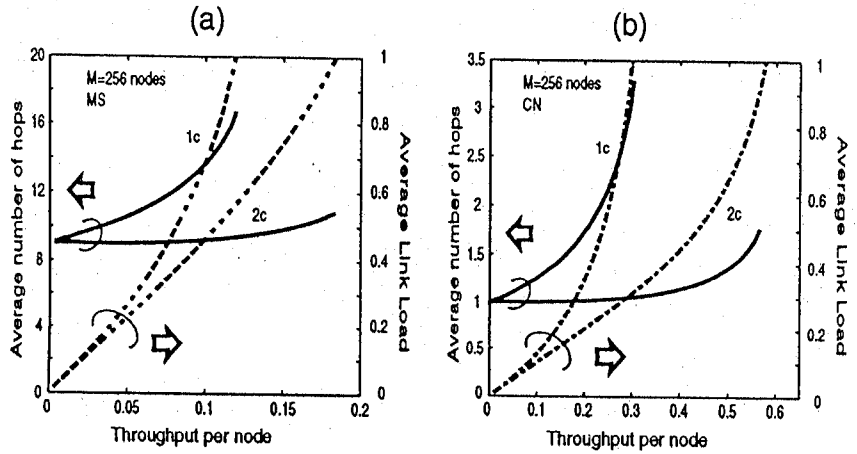

Fig. 2. Average number of hops and link load vs throughput in uniform traffic in (a) MS and (b) CN. $1c$ = no buffer, $2c$ = single-buffer.

Fig. 2 shows the average number of hops H and the link load u vs. throughput in uniform traffic for M=256 nodes for (a) MS [2] and (b) CN [5].

In the MS case, the average number of hops starts from a minimum of 9.02 and quickly increases with throughput. In the CN case, the average number of hops does not exceed 3.5 for the unbuffered ($1c$) case, and is below 2 for the buffered ($2c$) case. The strength of the centralized approach lies in the substantial decrease of the number of hops, which allows significantly lower power losses when the per-hop loss does not strongly depend on the number of stages, as when for instance alignment and fiber propagation losses dominate.

Also shown in the figure is the increase with throughput of the fraction of nonempty slots u, which causes an increase of the coherent crosstalk. For equal value of T, it is seen that u is much lower in CN.

3 Transmission

This section will derive the bit error rate $BER(n)$ of a packet that has hopped n times before reaching its destination. All symbols of interest are given in Table 1, along with the values used in the analysis.

Symbol	Meaning	Value/Range
M	# of nodes	256
u	link load	0–1
n	# of hops	1–1000
R	bit rate	1–20 Gb/s
B_o/R	norm. optical filter bandwidth	5
$\Delta F/R$	normalized sweep range	4
Δ_{MS}	node-node fiber span in MS	5 km
Δ_{CN}	node-node fiber span in CN	23 km
n_{sp}	EDFA spontaneous emission factor	1.3
P_{sat}	EDFA output saturation power	10 dBm
L_f	fiber loss (over Δ Km)	0.25*Δ (dB)
L_{hr}	header recognition tapping loss	1 dB
L_{al}	alignment loss	10 dB
L_{ad}	add/drop coupler loss	3 dB
x	# of crossbars in routing element	1 for 1c, 2 for 2c
L_r	routing block loss in MS	$3 * x$ (dB)
L_n	access node loss in CN	$L_{hr} * L_{ad}$
s	# of couplers crossed at the interconnect	$x * \log_2 M$
L_{ic}	interconnect loss (partial integration)	2*s (dB)
L_s	total loss at the star	$L_{hr} * L_{al} * L_{ic}$
α	switch crosstalk factor	-23 dB
N_x	# of crosstalk points	$n * x + 2$ for MS $n * s + 2$ for CN
P_{tx}	transmitted mark power	0 dBm in CN -1 dBm in MS
N_b	# bits/cell	1000

Table 1. Parameters used in calculations.

All transmitter lasers have a common nominal optical frequency $\nu_0 = \omega_0/2\pi$, and are externally On/Off keying (OOK) modulated with non-return-to-zero pulses at a bit rate $R = 1/T$, where T is the bit time. All TXs have the same power P_{tx} on mark and zero on space.

The direct-detection receiver consists of a bandpass optical filter of bandwidth B_o centered at the carrier frequency ν_0, a polarization filter, a photodiode (PD), and a matched (integrate-and-dump) filter, followed by a sampler and by the decision circuitry [6].

We fix the attention on a *tagged* bit of a cell taking n hops and reaching its intended receiver. It collects crosstalk at the routing switches and ASE noise in the optical amplifiers. The objective is to find the probability of error on such a bit.

3.1 Amplification: Distributed Network

Assume that nodes are regularly spaced Δ_{MS} km apart on a square grid. Two doped-fiber amplifiers A_1, A_2 are placed at the inputs of the node to compensate for fiber propagation loss and node power losses. We assume the amplifiers have power gain G and output saturation power P_{sat}. The ASE added at the output of each amplifier is modeled as an additive white gaussian

noise process with (one-sided) power spectral density $h\nu_0 n_{sp}(G-1)$ [1], where h is Planck's constant, and n_{SP} is the spontaneous emission factor.

To keep equal power levels in the network, the amplifiers are set to exactly compensate the per-hop loss:

$$G = L_{hr} L_{al} L_{ad} L_r L_f \tag{2}$$

where the losses are defined in Table 1.

With the aid of Fig. 1(a), the ASE power density accumulated by the test bit in *one* hop from point P to point P' of the following node is

$$N_{ase}(1) = h\nu n_{sp}(G-1)/(L_{hr} L_{al} L_{ad})$$

From Table 1 we get $N_{ase}(1) = 4.4 \times 10^{-19}$ W/Hz for 1*c* and $N_{ase}(1) = 8.8 \times 10^{-19}$ W/Hz for 2*c*. Given constraint (2), such noise contribution remains constant until absorption, and each hop contributes the same noise level, so that at the receiver $N_{ase}(n) = nN_{ase}(1)$. Optical filters of bandwidth B_o follow each amplifier to avoid saturation due to ASE.

If hopping packets are desired to have the same power level as newly injected packets, amplifier saturation also imposes a limit on the transmitted power:

$$P_{tx} L_{al} L_{hr} \leq P_{sat}\,.$$

Equality should be chosen to maximize the optical SNR.

3.2 Amplification: Centralized Network

If the nodes are regularly spaced Δ_{MS} km apart on a square grid, and the star is placed at the center of the square, the average fiber link length is approximately [7] $\Delta_{CN} \cong 0.28\sqrt{M}\Delta_{MS}$. To simplify the following analysis, all links are assumed to have the same length Δ_{CN}.

Doped-fiber amplifiers A_1, A_2, A_3 with saturation power P_{sat} are placed as in Fig. 1(b). To keep equal power levels in the network, the amplifiers are set to have unity roundtrip gain

$$G_1 G_2 G_3 = L_n L_f^2 L_s \tag{3}$$

where the losses are defined in Table 1. Amplifier A1 acts as a booster, with gain $G1 = P_{sat}/P_{rx}$, being P_{rx} the power in P. Amplifier A2 has gain $G2 = L_f * L_{hr} * L_{al}$, bringing the output power back to the saturation value. Finally A3 is chosen to satisfy (3).

With the aid of Fig. 1(b), the ASE power density accumulated by the test bit in *one* hop from point P to P' is seen to be

$$N_{ase}(1) = h\nu n_{sp}\left[\frac{(G_1-1)G_2G_3}{L_s L_f^2 L_n} + \frac{(G_2-1)G_3}{L_{ic} L_f L_n} + \frac{G_3-1}{L_f L_n}\right]$$

[1] Along the polarization direction of the signal.

since the ASE processes are independent. With the above value of the gains, we get

$$N_{ase}(1) = h\nu n_{sp}\left[\frac{(L_3-1)}{L_3} + \frac{(L_1-1)+(L_2-1)}{P_{sat}/P_{rx}}\right]$$

where $L_1 = L_f * L_{hr} * L_{al}$, $L_2 = L_{ic}$, $L_3 = L_f * L_n$. As before, given constraint (3), $N_{ase}(n) = nN_{ase}(1)$.

The position of the amplifiers and their gains have been selected so as to minimize $N_{ase}(1)/P_{rx}$ [2], subject to the unity gain constraint (3), and to the constraint that all power levels be below P_{sat}. The main design concept is to break up the lumped losses between amplifiers so as to balance them as much as possible.

For the values in Table 1, we get that for 1*c* the gains are $(G_1, G_2, G_3) = (13, 16.75, 12.75)$(dB), and $N_{ase}(1) = 8.54 \times 10^{-19}$(W/Hz); for 2*c* the gains are $(G_1, G_2, G_3) = (13, 16.75, 28.75)$(dB), and $N_{ase}(1) = 1.37 \times 10^{-17}$(W/Hz).

3.3 Photodetection

As the *tagged* cell hops from node to node, it collects crosstalk from the optical fields simultaneously crossing the same crossbar switches, and ASE noise at the amplifiers.

When it reaches its intended receiver after n hops, the complex envelope (with respect to the nominal frequency ν_0) of the optical field at the photodiode is $\tilde{e}_{rx} = \tilde{e}_0 + \tilde{e}_{xt} + \tilde{e}_{ase}$, where:

$\tilde{e}_0$ is the desired signal;

$\tilde{e}_{xt} = \sum_{i=1}^{n_{xt}} \tilde{e}_{xt}(i)$ is the accumulation of n_{xt} crosstalk interferers; and

$\tilde{e}_{ase}$ is the complex envelope of the accumulated ASE noise, which is an additive gaussian bandpass process of flat one-sided spectral density $N_{ase}(n)$ over the optical filter bandwidth B_o centered around ν_0.

The desired signal during the tagged bit time $(0 < t < T)$ is

$$\tilde{e}_0 = \sqrt{2P_{rx}}\, m_0 e^{j(\delta\omega_0 t + \phi_0)} \quad (\sqrt{\text{W}}) \tag{4}$$

where:

P_{rx} is the received mark power;

$m_0 = 1$ for mark, and zero for space;

ϕ_0 is a random variable (RV), uniform over $[-\pi, \pi]$ and constant over the bit time T, accounting for phase noise of the TX laser and other possible sources of phase uncertainty; assuming ϕ_0 constant over the bit time amounts to assuming that the TX laser linewidth is significantly smaller than the bit rate R;

$\delta\omega_0$ is a random frequency offset from the nominal carrier ω_0, uniform over $[-\pi\Delta F, \pi\Delta F]$. Such offset models a slow frequency drift of the TX laser, which could be obtained by modulating the laser current by a sawtooth sweep

[2] Such quantity, as shown in (17), is proportional to the inverse of the optical SNR.

signal or simply by loosely stabilizing the thermal drift of the laser. We impose $\Delta F < B_o - R$ to prevent the signal from drifting off the optical filter.

Each crosstalk interferer can be expressed as

$$\tilde{e}_{xt}(i) = \sqrt{2\alpha P_{rx}}\, m_i(t) \cos\Psi_i e^{j(\delta\omega_i t + \phi_i)} \quad (\sqrt{\mathrm{W}}) \tag{5}$$

where:

$\delta\omega_i$ and ϕ_i are independent, identically distributed (IID) RVs, with the same statistics as $\delta\omega_0$ and ϕ_0, respectively;

$m_i(t) \in \{0,1\}$ represents the OOK modulation of the interferers, and the dependency on time accounts for the random bit-misalignment of the various OOK channels.

$\alpha \ll 1$ is the power crosstalk factor of each crossbar. All crosstalk interferers have the same power, since conditions (2) and (3) impose that cells that meet at a crossbar have the same power level, no matter how many hops they have taken [3].

$\cos\Psi_i$ is the polarization component of the i-th interferer along the polarization direction of the tagged cell. The angles Ψ_i are assumed to be independent RVs, uniform over $[-\pi, \pi]$. Although a practical receiver will not keep track of the desired signal's polarization state, neglecting orthogonal (non-coherent) components has little impact on performance, since the crucial crosstalk contribution is the coherent beat with the signal.

The input field can be rewritten as

$$\tilde{e}_{rx} = \sqrt{2P_{rx}}\, e^{j(\delta\omega_0 t + \phi_0)} [m_0 + \tilde{x}(t) + \tilde{a}(t)] \tag{6}$$

where the normalized crosstalk field is

$$\tilde{x} = x_i(t) + j x_q(t) = \sqrt{\alpha} \sum_{i=1}^{n_{xt}} m_i(t) \cos\Psi_i e^{j(\Delta\omega_i t + \Phi_i)} \tag{7}$$

where $\Delta\omega_i = \delta\omega_i - \delta\omega_0$ and $\Phi_i = \phi_i - \phi_0$.

The normalized ASE field is

$$\tilde{a}(t) = a_i(t) + j a_q(t) = \frac{\tilde{e}_{ase}(t)}{\sqrt{2P_{rx}}} e^{-j(\delta\omega_0 t + \phi_0)}. \tag{8}$$

The current after the photodetector is

$$i(t) = I_p(t) + i_{sn}(t) + i_{th}(t) \tag{9}$$

where $I_p(t) = \frac{\mathcal{R}}{2}|\tilde{e}_{rx}(t)|^2$, $\mathcal{R}$ is the responsivity of the photodetector (A/W). Since the received power is large, we neglect both the shot noise current and the thermal noise of the electronic circuitry.

During a mark signal bit, I_p can be written as

$$I_p = \mathcal{R} P_{rx} \{1 + n_{s-xt} + n_{s-sp} + n_{xt-xt} + n_{xt-sp} + n_{sp-sp}\} \tag{10}$$

[3] This is true if the extra power due to accumulation of crosstalk and ASE on a cell can be neglected

where the contributions of the beat terms between signal and crosstalk (s-xt), signal and ASE (s-sp), crosstalk with itself (xt-xt), crosstalk with ASE (xt-sp), and ASE with itself (sp-sp) are

$$\begin{aligned} n_{s-xt}(t) &= 2x_i(t) \\ n_{s-sp}(t) &= 2a_i(t) \\ n_{xt-sp}(t) &= 2[x_i(t)a_i(t) + x_q(t)a_q(t)] \\ n_{xt-xt}(t) &= x_i^2(t) + x_q^2(t) \\ n_{sp-sp}(t) &= a_i^2(t) + a_q^2(t). \end{aligned} \tag{11}$$

In the following we will neglect all noise terms other than n_{s-sp} and n_{s-xt} which are by far the dominating terms.

The normalized statistic at the decision gate can be expressed as

$$Z = \left(\frac{1}{\mathcal{R}P_{rx}}\right) \frac{1}{T} \int_0^T i(t)\, dt = 1 + Y_{s-xt} + Y_{s-sp} \tag{12}$$

where $Y_{s-xt} = \frac{1}{T}\int_0^T n_{s-xt}(t)dt$, and $Y_{s-sp} = \frac{1}{T}\int_0^T n_{s-sp}(t)dt$.

As the number of IID crosstalk interferers n_{xt} gets large, the distribution of Y_{s-xt} tends, by the central limit theorem, to a gaussian RV. Hence the BER can be approximated by a gaussian formula [9].

Since the noise level during a zero is much lower than the noise level during a one, in the gaussian assumption we approximate

$$\mathrm{BER}(n) \cong \mathrm{Q}\left(\frac{1}{\sqrt{\sigma_{s-xt}^2 + \sigma_{s-sp}^2}}\right) \tag{13}$$

where $\mathrm{Q}(x) = \frac{1}{\sqrt{2\pi}}\int_x^\infty e^{-y^2/2}\, dy$, and $\sigma_\bullet^2$ denotes variance of $Y_\bullet$.

Signal-crosstalk beat – The Appendix shows that $x_i(t)$ and $x_q(t)$ are uncorrelated and have the same autocorrelation

$$R_{x_i}(\tau) = \mathrm{E}[x_i(t)x_i(t+\tau)] = \frac{\alpha\,\mathrm{E}[n_{xt}]}{4} \mathrm{sinc}^2(\Delta F\tau)\, R_m(\tau) \tag{14}$$

The autocorrelation of the OOK asynchronous modulation signals $m_i(t)$ is [11]: $R_m(\tau) = \frac{1}{4}(1 + \Lambda(\frac{\tau}{T}))$ [4]. For bit-aligned cells we have $R_m(\tau) = 1/2$.

The variance of Y_{s-xt} is calculated as $\sigma_{s-xt}^2 = \frac{4m_0}{T^2}\int_0^T\int_0^T R_{x_i}(\beta-\alpha)d\alpha\, d\beta$. A closed form of this double integral can be found, giving:

$$\boxed{\sigma_{s-xt}^2 = \frac{\mathrm{E}[n_{xt}]}{2}\alpha\,\eta(\rho)} \tag{15}$$

where $\rho = 2\pi\Delta F/R$, and the beat efficiency factor $\eta(\rho)$ equals

$$\eta(\rho) = \begin{cases} \frac{2}{\rho^2}\left(-3\gamma_e - 3\ln(\rho) + 3\mathrm{Ci}(\rho) + 2\rho\mathrm{Si}(\rho) - 1 + 2\cos(\rho) - \mathrm{sinc}(\rho/\pi)\right) & \text{asynch.} \\ \frac{4}{\rho^2}\left(-\gamma_e - \ln(\rho) + \mathrm{Ci}(\rho) + \rho\mathrm{Si}(\rho) - 1 + \cos(\rho)\right) & \text{synch.} \end{cases} \tag{16}$$

[4] The triangular function is defined as $\Lambda(\frac{t}{x}) = 1 - |t|/x$ for $|t| < x$ and zero outside.

where $\gamma_e = 0.5772...$ is euler's gamma, and $\mathrm{Si}(\rho)$ and $\mathrm{Ci}(\rho)$ are the sine and cosine integrals, respectively [12]. For large ρ, in both cases we have $\eta(\rho) \cong 2\pi/\rho$.

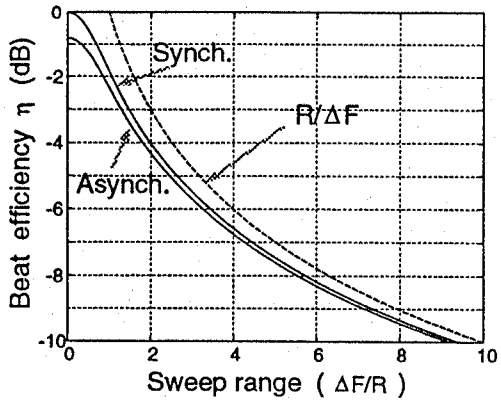

Fig. 3. Beat efficiency η vs normalized sweep range $\Delta F/R$.

Fig. 3 shows η vs. the normalized sweep range $\Delta F/R$. It is seen that both the bit-aligned and the asynchronous curves quickly converge to $R/\Delta F$. For the asynchronous case, $\eta(0) = 5/6$. From (15) one can see that, when the term s-xt dominates, one can trade $\Delta\alpha$ dBs in the switch crosstalk factor for $\Delta\eta$ dBs in the beat efficiency by acting on the sweep range $\Delta F/R$.

Signal-ase beat – From (8) we can rewrite $\tilde{a}(t) = \tilde{n}(t)\, e^{-j\delta\omega_0 t}$, where $\tilde{n} = n_i + jn_q$ is a lowpass zero-mean complex gaussian process, and where n_i and n_q are uncorrelated, with the same spectral density [5] $S_{n_i}(f) = \frac{N_{ase}(n)}{2P_{rx}} \Pi(\frac{f}{B_o})$.

The term $w(t) = e^{-j\delta\omega_0 t}$ is recognized as a frequency modulation, so that we get [10]: $R_w(\tau) = \mathrm{E}\{w(\tau)\} = \mathrm{sinc}(\Delta F\tau)$ and therefore the spectrum $S_w(f) = \frac{1}{\Delta F}\Pi(\frac{f}{\Delta F})$.

Since the probability density of $\delta\omega_0$ is symmetric around zero, one finds that the real and imaginary part of $\tilde{a}$, a_i and a_q, are also uncorrelated and have identical spectrum

$$S_{a_i}(f) = S_{n_i}(f) \otimes S_w(f)\,,$$

where $\otimes$ indicates convolution. Such convolution has value $\frac{N_{ase}(n)}{2P_{rx}}$ for $|f| < (B_o - \Delta F)/2$, and linearly decreases to zero for $(B_o - \Delta F)/2 < |f| < (B_o + \Delta F)/2$.

Now, $a_i(t)$ is filtered by the integrator of noise bandwidth $R/2$. Since we imposed $B_o - \Delta F \geq R$, the result is essentially the same as if $n_i(t)$ only

[5] The rectangular function is defined as $\Pi(\frac{t}{x}) = 1$ for $|t| < x/2$ and zero outside.

were filtered, i.e., the multiplying exponential term in (8) has no effect on the variance of the term n_{s-sp}, which simply is

$$\boxed{\sigma^2_{s-sp} \cong 2\frac{N_{ase}(1)}{P_{rx}} nR} \qquad (17)$$

4 Combining Teletraffic and Transmission

The system parameters used in this results section are given in Table 1, unless otherwise noted.

Assuming cells of N_b bits, the unconditional packet error rate is obtained by conditioning on the number of hops n taken by a typical packet in the network as

$$PER = \sum_{n=1}^{\infty} [1 - (1 - BER(n))^{N_b}] p_h(n) \qquad (18)$$

where $p_h(n)$ is the probability mass function of the number of hops h [2][5]. Since noises are not uncorrelated bit-by-bit, (18) is indeed an upper-bound.

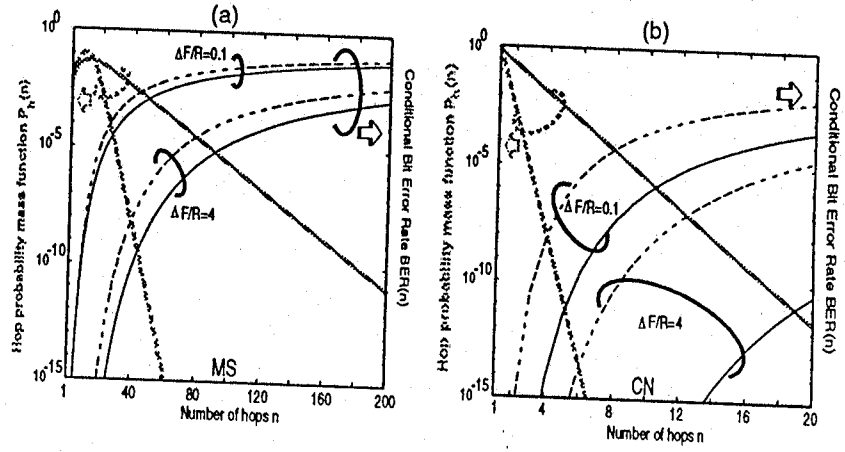

Fig. 4. $BER(n)$ and hop distribution $p_h(n)$ vs hop number n in (a) MS and (b) CN for a fixed throughput $T = 0.12$ and bit rate R=20 Gb/s. Sold: no buffer 1c; Dotted: single buffer 2c.

Fig. 4 shows the two key variables of eq. (18), namely, conditional bit error rate BER(n) and hop-distribution $p_h(n)$. Dotted lines refer to 2c elements, and solid lines to 1c elements. The curves are for (a) MS and (b) CN, for a fixed throughput $T = 0.12$ and bit rate $R = 20Gb/s$. As seen in Fig. 2, this is the maximum throughput T achievable with MS1c at full load ($u = 0.99$). At this

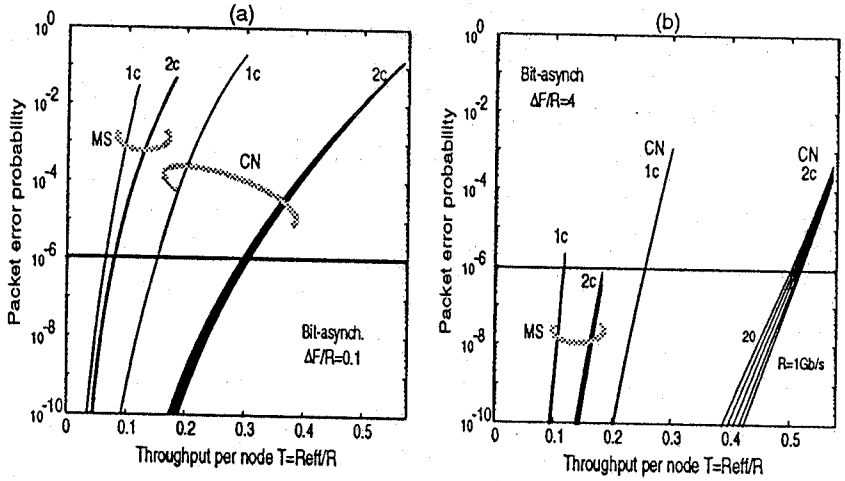

Fig. 5. PER vs throughput in MS and CN for (a) low sweep ($\Delta F/R = 0.1$); and (b) substantial sweep ($\Delta F/R = 4$).

value of T, MS2c has $u = 0.56$, CN1c has $u = 0.16$, and CN2s has $u = 0.12$. Such lower loads allow lower values of crosstalk.

Interestingly, the slope of the hop-distribution curves is almost 10 times steeper in CN, due to its weakly-multihop nature. However, since the per-hop power losses (and hence the ASE due to their compensation by optical amplification) are much larger in CN, the BER(n) curves grow much faster with n. Sweeping the optical carrier across almost all of the optical filter bandwidth ($B_o = 5R$) using $\Delta F/R = 4$ is beneficial in all cases where signal-crosstalk beat dominates. The curve for CN 1c with $\Delta F/R = 4$ is out of range in Fig. 4(b).

PER vs throughput curves are given in Fig. 5, with R ranging from 1 to 20 Gb/s. For a given transmitter bit rate R, T indicates the actual sustained rate R_a at the access node, since $T = R_a/R$.

In Fig. 5(a) there is essentially no frequency sweeping, $\Delta F/R = 0.1$, while in 5(b) there is substantial sweeping, $\Delta F/R = 4$. It is seen that, notwithstanding the poor crosstalk factor $\alpha = -23$ dB, using the sweeping technique allows good network performance, since the effective crosstalk factor is $\eta\alpha \cong -30$ dB. All curves depend very weakly on R, indicating that coherent crosstalk is the dominant impairment, which, as seen from (15), is bit rate independent. Therefore they mostly improve with sweeping, as seen in Fig.5(b).

Clearly, the weakly-multihop CN can sustain much larger throughputs at lower error rates than the intrinsically-multihop MS. However, some form of flow-control is needed in CN to avoid unacceptably large error rates at high loads.

5 Conclusions

This work compares intrinsically-multihop to weakly-multihop topologies for space-division transparent optical networks with deflection routing.

The better connectivity provided by the centralized network allows less congestion to build up for the same sustained throughput, and therefore less crosstalk and less deflections. Centralized networks therefore can sustain larger throughputs at lower error rates than distributed, intrinsic-multihop topologies.

A frequency sweeping technique has been shown to greatly alleviate the impact of coherent crosstalk, thereby allowing network operation with crosstalk factors around $-20dB$. In the centralized network, however, a control of the network load is necessary to avoid excessive error rates at the receiver.

Another way of decreasing both coherent crosstalk and deflections is to deplete the optical transport layer by using faster transmitters/receivers, thus supporting the same amount of traffic at lower loads. When this is done, less complicated, unbuffered structures (1c) are more desirable than more efficient, more lossy buffered structures (2c). This shifts the cost burden to speed-up the optical transmitter/receiver at the access node to allow major simplifications and cost reductions of the optical transport/switching part of the network.

Appendix

This appendix will derive the cross- and auto-correlation of the crosstalk components x_i, x_q defined in (7). We have:

$$R_{x_i x_q}(\tau) = \mathrm{E}[\alpha \textstyle\sum_{i=1}^{n_{xt}} \sum_{j=1}^{n_{xt}} \mathrm{E}[m_i(t)m_j(t+\tau)\cos\Psi_i \cos\Psi_j \cdot \\ \cdot \cos(\Delta\omega_i t + \Phi_i)\sin(\Delta\omega_j(t+\tau)+\Phi_j)/n_{xt}]]$$

where the outer expectation on the RHS is taken with respect to n_{xt}. All terms with $i \neq j$ average to zero because $\mathrm{E}[\cos\Psi_i] = 0$, being Ψ_i uniform and independent of n_{xt}. Considering that $\mathrm{E}[m_i(t)m_i(t+\tau)] \triangleq R_m(\tau)$ for all i's, and that $\mathrm{E}[\cos^2(\Psi_i)] = 1/2$, we have

$$R_{x_i x_q}(\tau) = \mathrm{E}[\alpha \sum_{i=1}^{n_{xt}} R_m(\tau)\frac{1}{2}\mathrm{E}\left[\frac{\sin\Delta\omega_i\tau + \sin(\Delta\omega_i(2t+\tau)+2\Psi_i)}{2}\right]] = 0$$

because for all i's $\mathrm{E}[\sin\Delta\omega_i\tau] = 0$, since the probability density function (pdf) of $\Delta\omega_i$ is symmetric around zero, and $\mathrm{E}[\sin(\Delta\omega_i(2t+\tau)+2\Psi_i)] = 0$ because $2\Psi_i$ is uniform.

Analogously,

$$R_{x_i}(\tau) = \mathrm{E}[\alpha \textstyle\sum_{i=1}^{n_{xt}} \sum_{j=1}^{n_{xt}} \mathrm{E}[m_i(t)m_j(t+\tau)\cos\Psi_i \cos\Psi_j \cdot \\ \cdot \cos(\Delta\omega_i t + \Phi_i)\cos(\Delta\omega_j(t+\tau)+\Phi_j)/n_{xt}]] \\ = \mathrm{E}[n_{xt}]\alpha R_m(\tau)\tfrac{1}{2}\textstyle\sum_i \mathrm{E}\left[\frac{1}{2}\cos\Delta\omega_i\tau\right]$$

This establishes (14), by noting that $\mathrm{E}[e^{j\Delta\omega_i\tau}] = \mathrm{E}[\cos\Delta\omega_i\tau] = \mathrm{sinc}^2(\Delta F\tau)$, being this the characteristic function of the RV $\Delta\omega_i$, i.e., the Fourier transform of its triangular-shaped pdf $\frac{1}{\pi\Delta F}\Lambda(\frac{\Delta\omega}{2\pi\Delta F})$.

- **Evaluation of $\mathrm{E}[n_{xt}]$** Let C be the number of hops added by each deflection. For CN C=1, while for MS C=4 [4]. Let H_{min} be value of the the average number of hops at low load, when no deflections occur (see Fig. 2). Given a path of n hops, we approximate the number of deflections along the path as $n_d = \lfloor \frac{max(n-H_{min},0)}{C} \rfloor$. Since a deflection occurs when a packet meets x competing packets at a routing element ($x = 1$ for 1c and $x = 2$ for 2c), on a path of n hops there are *at least* $x \cdot n_d$ crosstalk interferers. Let N_x be the number of points along the path where crosstalk may arise (*crosstalk points*, see Table 1). If we assume that at the $N_x - x \cdot n_d$ points where deflection does not occur an interferer is present with probability u (the link load defined in section 2), then $\mathrm{E}[n_{xt}] = x \cdot n_d + u(N_x - (x \cdot n_d))$.

References

[1] E. L. Goldstein and L. Eskildsen, "Scaling limitations in transparent optical networks due to low-level crosstalk," *IEEE Photon. Technol. Lett.*, vol. 7, pp. 93–94, Jan. 1995.

[2] F. Forghieri, A. Bononi, and P. R. Prucnal, "Analysis and comparison of hot-potato and single-buffer deflection routing in very high bit rate optical mesh networks," *IEEE Trans. Commun.*, vol. 43, pp. 88–98, Jan. 1995.

[3] P. Baran, "On distributed communications networks," *IEEE Trans. Commun. Syst.* vol. 12, pp. 1–9, Mar. 1964.

[4] N. F. Maxemchuk, "Comparison of deflection and store-and-forward techniques in the Manhattan Street and Shuffle-Exchange networks," in *Proc. IEEE INFOCOM '89*, pp. 800–809, Apr. 1989.

[5] A. Bononi, "Space-division optical star networks with deflection routing," *30th Annual Conference on Information Science and Systems*, session FA-1, Princeton, NJ, March 20–22, 1996.

[6] O. K. Tonguz and L. G. Kazovsky, "Theory of direct-detection lightwave receivers using optical amplifiers," *IEEE J. Lightwave Technol.*, vol. 9, pp. 174–181, Feb. 1991.

[7] O. K. Tonguz and K. A. Falcone, "Fiber-optic interconnection of local area networks: physical limitations of topologies," *IEEE J. Lightwave Technol.*, vol. 11, pp. 1040–1052, May/June 1993.

[8] A. Bononi, "Combined teletraffic/transmission analysis of a transparent space-division optical star network," in *Proc. IEEE GLOBECOM '96*, London, Nov. 1996.

[9] P. A. Humblet and M. Azizoglu, "On the bit error rate of lightwave systems with optical amplifiers," *IEEE J. Lightwave Technol.*, vol. 9, pp. 1576–1582, Nov. 1991.

[10] A. Papoulis: "Probability, random variables and stochastic processes." McGraw-Hill 1984 Second edition, p. 228-230.

[11] — ibid., pp. 321.

[12] M. Abramowitz, I. A. Stegun: "Handbook of mathemtical functions." Dover 1970, p. 231.

Ultrafast All-Optical Signal Processing for Packet Switching

D. Cotter, M. C. Tatham, J. K. Lucek, M. Shabeer,
K. Smith, D. Nesset, D. C. Rogers and P. Gunning

BT Laboratories, Martlesham Heath, Ipswich, Suffolk IP5 7RE, UK
david.cotter@bt-sys.bt.co.uk

Abstract

Recent advances in the development of 100 Gbit/s self-routing packet networks are described. The most practical design approach currently is to use very simple and sparse processing in the ultrafast domain, relying on only a small number of photonic devices with primitive functionality. The development of suitable address coding ('keyword' coding), ultrafast word recognition, and a new self-routing protocol ('dead reckoning') makes it possible to obtain efficient routing in ultrafast mesh networks with massive throughput and speed, yet requiring a minimal amount of bit-level processing.

1. Introduction

We are exploring ways of developing ultrafast photonic networks capable of supporting multi-Gbit/s interconnections in future distributed computing environments, with very fast response and low latency [1]. As well as campus- and local-area networks (Fig. 1), ultrafast technologies will find a role in the communications backbone of multi-processor systems, and potentially also at the heart of future massive-capacity routers and servers. Such networks will be radically different from the networks of today, which are burdened with ponderous signalling protocols and buffering at routing switches. One of the options we are developing is a photonic self-routed network, using fixed-length packets composed of picosecond optical pulses at rates around 100 Gbit/s [2–4]. The packets are routed through the network on all-optical pipes, with header data processing 'on the fly' using ultrafast photonic logic, and with no or very minimal buffering in the optical domain.

A basic stability criterion for such a network is that each routing decision made 'on the fly' within the network must be completed within the transmission time for a single packet (e.g. a few nanoseconds for a ~500-bit packet length at 100 Gbit/s) and therefore must be as simple as possible. A routing decision involves processes at two distinct levels of granularity—the bit level and the packet level. In ultrafast networks, processes at the bit level require photonic devices with response